Interference on Static Energy Meters Resulting From Droop of the Current Transformer

Bas ten Have, *Member, IEEE*, Leonardo Bolzonella, Tom Hartman, *Member, IEEE*, Niek Moonen, *Member, IEEE*, Frank Leferink, *Fellow, IEEE*

***Abstract*—Robust energy measurements for household consumption billing is important for consumer confidence. Recent studies have shown electromagnetic interference problems with static energy meters, this results in incorrect billing. The interfering current waveforms are pulsed currents with a short pulse duration, fast rising slope, and large crest factor. These kind of waveforms are largely present in modern low-voltage networks. The root-cause of the interference on static energy meters that use a Rogowski coil is known, however for meters that use a current transformer as their current sensing element this is unknown, while those meters contribute to errors up to 200%. Therefore, this article researches the root-cause of interference on static energy meters that use the current transformer principle for current sensing. It was found that the current transformer exhibits droop and the current pulses to be measured are not properly reconstructed. As a result, when the power/energy is calculated errors occur. This explains why current transformer based static energy meters are prone to electromagnetic interference.**

***Index Terms*—Current transformer, droop, electromagnetic interference, pulsed currents, static energy meters.**

I. Introduction

FOR CONSUMER confidence it is important to have trustworthy energy consumption billing. Energy billing is done using static energy meters, which are currently widely deployed throughout the European Union (EU) [1], these are electronic meters and replace conventional electromechanical (or Ferraris) meters. Together with the surging energy prices [2], the meter renewal has increased customer awareness reliable energy billing. Furthermore, recent studies have shown electromagnetic interference (EMI) problems with static energy meters resulting in incorrect measured consumptions. These are, among others, due to harmonic disturbances [3], photovoltaic installations [4], various modern appliances [5], dimmed lighting equipment [6], a water pump for fish ponds [7], and multimedia equipment [8]. Which were researched based on consumer reports of incorrect billed consumptions. These showed energy consumption errors up to +2675% for the water pump [7], and a perceived energy generation of 600 W for the multimedia equipment when actually energy was being consumed [8]. The interfering current waveforms being drawn are non-linear and have a pulsed nature with a short pulse duration, fast rising slope, and large crest factor, as became clear from a parametric comparison of those waveforms in [9].

The root-cause of the interference on static energy meters is mostly unknown, because the static energy meter was treated as a black-box. However, information is known on the current sensing element inside the interfered meters. To sense the current different techniques are used, which are: current transformer (CT), Hall effect sensor, Rogowski coil, and shunt resistor. Those techniques are explained in detail in [10]. All of these sensors give an output voltage relative to the current. In [9] it was already evidenced that the highest interference created was by Rogowski coil meters, CT meters also gave notable errors (up to 200%), while the Hall effect sensor and shunt resistor have shown minor errors. The root-cause for Rogowski coil based meters was already found in [11]. Clipping of the amplifier at the output of the Rogowski coil due to the high rise times of the interfering waveforms and the Rogowski coil being a differential current sensor. The root-cause for CT based meters is however unknown. And not the same as the Rogowski coil meters.

Energy metering using CTs was previously examined in [12]. It was found that a discrepant response, due to droop of the CT when measuring pulsed currents, resulted in interfered energy measurements. Droop refers to the decreasing sense voltage when a current pulse with a large constant part is applied at the primary side [10], as is the case for a square-wave. Droop problems with transformers are not uncommon as [13] showed this effect for fast rise time pulse transformers, and [14] showed droop of CTs for current sensing in switched-mode power converters. Still, problems were not foreseen for static energy meters.

Therefore, the aim of this article is to show the root-cause of the interference on static energy meters that use the CT principle as their current sensing principle. This is done by analysing the response of a CT by simulations and measurements under different loading conditions representative for the on-site situation. Afterwards, these findings are used to determine the implications for energy metering of the static energy meter under test.

This article is structured as follows: Section II analyses the EMI problems on static energy meters. In Section III the internals of the static energy meter under test are described. Then the methodology to simulate and measure the response of the CT and the implications for energy metering is shown in Section IV. Afterwards, the response of the CT as embedded inside the static energy meter with different non-linear test waveforms is shown in Section V. And Section VI shows the

Bas ten Have, Leonardo Bolzonella, Tom Hartman, and Niek Moonen are with the University of Twente, Enschede, The Netherlands (e-mail: bas.tenhave@utwente.nl; l.bolzonella@student.utwente.nl; tom.hartman@utwente.nl; niek.moonen@utwente.nl).

Frank Leferink is with the University of Twente, Enschede, The Netherlands, and also with THALES Nederland B.V., Hengelo, The Netherlands (e-mail: leferink@ieee.org).

implications of these responses on the energy measurements by the static energy meter under test. Finally, Section VII concludes this article.

II. Analysis of the EMI Problem

A. Interference Waveforms

Several cases of EMI on static energy meters based on consumer complaints were listed in the introduction. Using a parametric waveform model the relevant error inducing features from the waveforms were extracted in [9], those relevant parameters are summarized in Table I. From this overview it is clear that the interfering waveforms represent small pulsed current waveforms with a relatively high crest factor and a fast rise time, consequently those pulses also have a low charge. A representative waveform both in terms of shape and waveform parameters is shown in Fig. 1. This waveform is drawn by a speed-controlled water pump and was found to interfere with static energy meters based on consumer complaints [7]. It represents a wide-band signal, i.e. the current harmonics up to 2 kHz are quite significant compared to the fundamental frequency of 50 Hz. Additionally, the frequency content above 2 kHz is reaching up to 10% of the current amplitude at the fundamental frequency. In contrast, for the voltage only the component at the fundamental frequency has a significant contribution.

TABLE I. Critical ranges of time-domain parameters found to result in interference of static energy meters [9].

Parameter	Critical range
Charge	4-8 mC
Crest factor	> 5
Pulse width	0.2-1.2 ms
Rising slope	> 0.1 A/µs

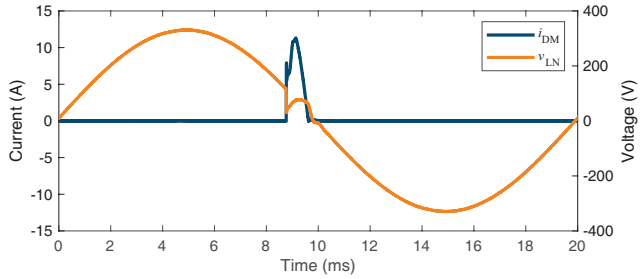

(a) Time-domain response

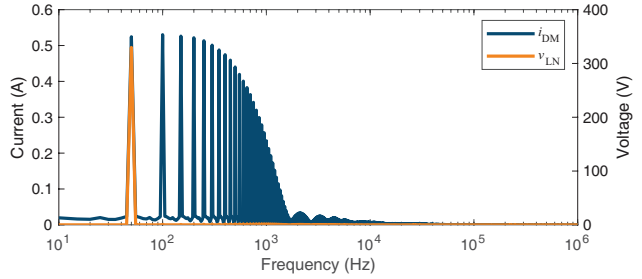

(b) Frequency-domain response

Fig. 1. Waveforms from a speed-controlled water pump resulting in EMI problems with static energy meters [7].

Using two on-site studies it was found that those interfering waveforms are representative for the actual residential grid. First, an extensive study on the waveforms from individual appliances that are typically connected in a residential grid showed that 43% of the surveyed equipment has parameters inside the critical range related to the static energy meter interference [15]. Second, the waveforms that occur at the meter connection point are surveyed in [16] at representative sites including modern sites that include an electric vehicle (EV) charging station and a photovoltaic (PV) installation. Many non-linearities are found and the on-site current waveforms show similarities with the interference waveforms. In 74% of the on-site waveforms critical parameters are found. And thus the static energy meters are exposed to EMI. An example of a representative on-site waveform is shown in Fig. 2. It shows a superposition of a linear and a non-linear pulsed waveform. The slope of this waveform is 0.17 A/µs, which is within the critical range.

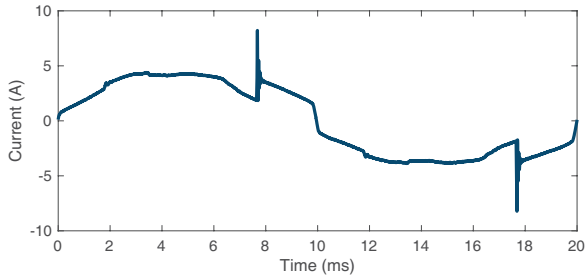

Fig. 2. Waveform obtained during the on-site survey of waveforms occurring at the meter connection point in [16].

B. Shortcomings in Standardization

Based on these studies the shortcomings in standardization were pinpointed in [17]. Where it was shown that the harmonized standards that are used to demonstrate a proper functioning of the product according to the EU legalization only focus on sinusoidal or chopped-sinusoidal signals, i.e. only cover one or a very narrow-band of frequencies at once. Such as the IEC 62053-21 [18] for electricity metering equipment including limits for harmonic voltages and currents, and the IEC 61000-4-19 [19] for conducted differential mode disturbances which covers frequency swept continuous-wave signals. In fact, such frequency domain tests based on single tone signals that aim to determine the system's transfer function cannot be used as those only hold for linear time-invariant systems, which the residential system is not, due to non-linear and time-varying elements present in the system [20]. Accordingly, this shows that the features of the interference waveforms are not sufficiently covered in the current standardization framework.

As this article aims at researching the root-cause of the interference problem, in the context of CT based static energy meters. Pulsed currents based on the actual on-site case are used to prove the susceptibility of the CT measurement, rather than the test signals as included in the harmonized test standards.

III. Inside the Static Energy Meter

A. Static Energy Meter Circuitry

The printed circuit board (PCB) of the static energy meter under test is shown in Fig. 3(a). The voltage is sensed using a resistive voltage divider and the current is sensed using the CT principle. The CT as used by the static energy meter is a model 4629X017 as manufactured by Vacuumschmelze, and is shown in Fig. 3(b). The CT has a 3 dB bandwidth from 5 Hz till 14 kHz, as is measured using a frequency response analysis with a Picoscope 5444D digital oscilloscope, the obtained Bode plot is shown in Fig. 4. The static energy meter under test uses a Renesas M16C/6C microcontroller unit (MCU) for processing.

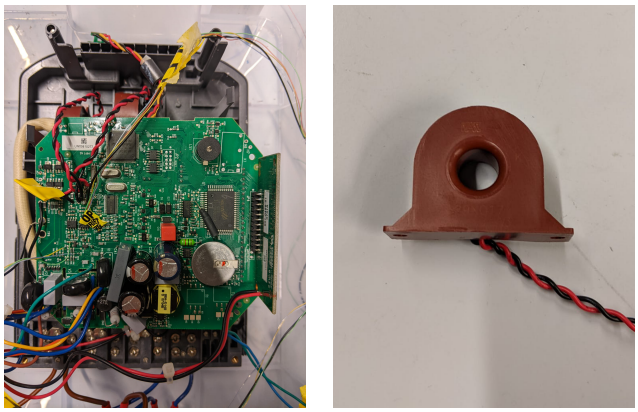

(a) PCB with added probe points (b) CT

Fig. 3. Internals of the static energy meter.

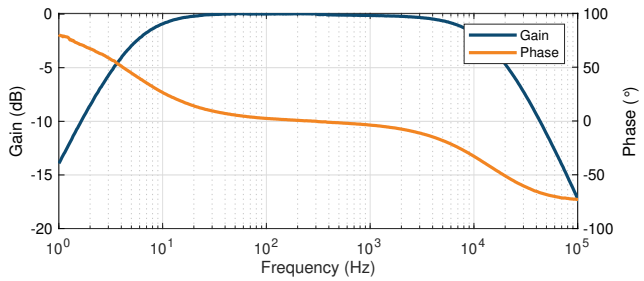

Fig. 4. Bode plot of the CT inside the static energy meter.

B. Current Sensing Method

The schematic of the current sensing method is shown in Fig. 5. It includes the magnetisation inductance, L_e, and the secondary winding resistance, R_s, to model the behavior of the CT [21]. The varying magnetic field in the primary coil induces a current in the secondary coil. To produce a flux in a CT's core for a finite permeability, a supporting current is needed, called the magnetization current [21]. This is modelled by a magnetisation inductance. It is determined by the dimensions and permeability of the core material [22]. This inductance is ideally infinite (i.e. infinite permeability), and tends to zero when the core saturates [23]. The secondary winding resistance is modelled by R_s. The L_e and R_s are determined using a Hameg HM8118 LCR bridge and are 1.69 H and 42.8 Ω, respectively. The secondary coil is then the input of a transimpedance amplifier (TIA), converting the current into a measurable voltage by the MCU. It amplifies the signal with a factor 32.25 and adds a low-pass filter with a cut-off frequency of 60 kHz.

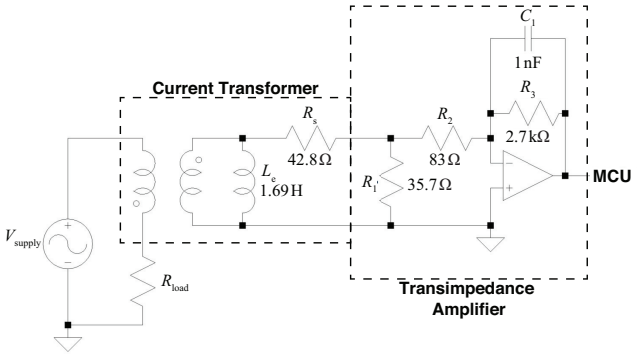

Fig. 5. Schematic of the current sensing method used by the CT.

IV. Methodology

A. Simulation of the CT Response

1) Simulation circuit: First, the response of the CT is simulated in LTspice. In order to avoid effects of the TIA on the response of the CT its behavior is mimicked by using the equivalent resistance (R_{eq}) in simulation, which is similarly to using a burden resistance. The equivalent resistance of the TIA is 24.1 Ω, as was found during simulation of the circuit with TIA in LTspice. The current induced in the secondary winding of the CT is modelled using a current source (i_s). The simulation circuit is shown in Fig. 6. This simulation circuit properly represents the behavior of the actual CT as shown in [24].

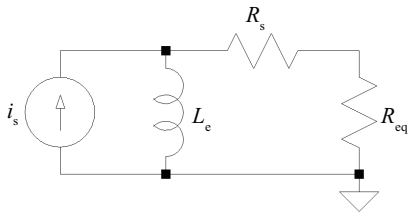

Fig. 6. Simulation circuit representing the CT.

2) Test waveforms: As was indicated in Section II, the waveforms that contribute to interference on static energy meters are typically characterized by trapezoidal pulses [9]. Therefore, the test waveforms used for simulation are trapezoidal pulses with parameters inside the critical range from Table I. All test waveforms use a fundamental frequency of 50 Hz, i.e. the repetition frequency of the pulses, as it represents waveforms at mains frequency. A peak value of 10 A is used as the analysis in [9] found that the interfering currents are close to this value. Four different test waveforms are used in simulation, an overview of these test waveforms is provided in Table II and visualized in Fig. 7. *Wave 1* is a 50% duty cycle square-wave that is used to simulate the CT

behavior with a relatively simple pulsed waveform. *Wave 2* represents a simplified representation of the interference currents as described in Section II. *Wave 3* represents the bipolar version of *Wave 2* as [9] showed that both uni- and bipolar signals can cause interference on static energy meters. *Wave 4* represents another variation of *Wave 2* where the top part of the pulse is not constant but is superimposed with a chopped 1 kHz sinusoidal wave. This is done to represent a waveform more closely resembling on-site waveforms, e.g. the pulse from Fig. 1(a) also does not have a flat top. Besides, it is known that droop occurs for constant parts of the signal which is not the case now.

TABLE II. Test waveforms for simulation.

#	Polarity	Pulse width [ms]	Rise/fall time [µs]
Wave 1	Uni	10	1
Wave 2	Uni	1	1
Wave 3	Bi	1	1
Wave 4	Uni	1	1

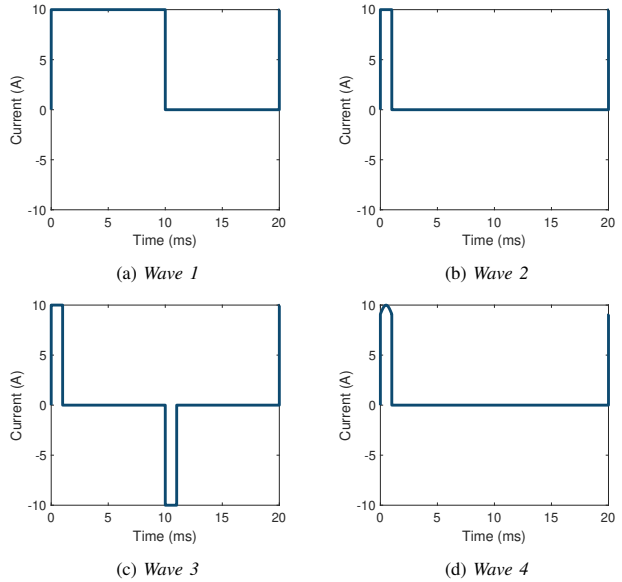

(a) *Wave 1* (b) *Wave 2*

(c) *Wave 3* (d) *Wave 4*

Fig. 7. Visualization of the test waveforms used for simulation of the CT response.

3) Circuit parameters: When there is no change in primary current, as is the case at the top and bottom of the square-waves that are used as test waveforms, no current will be induced on the secondary winding of the CT. The output voltage of the CT will drop exponentially dependent on the time constant, τ, of the circuit, Fig. 6, according to (1). This behavior is called droop. During simulation different values for the time constant are investigated by changing L_e. Table III lists the component values during simulation. Similar changes in time constant (and thus similar simulation results) can be achieved by changing either R_s or R_eq, e.g. by changing the burden resistor of the circuit. In order to limit the droop effects the time constant should be large compared to the pulse length to minimize the error [14]. *Sim 1* represents an ideal CT with a high L_e (large time constant). *Sim 2* represents the actual CT under test. *Sim 3* represents the situation where the current returns to zero considering a 50 Hz 50% duty cycle square wave ($\geq 5\tau$). And *Sim 4* is representative for a worst case scenario (very low time constant).

$$\tau = \frac{L_\mathrm{e}}{R_\mathrm{s} + R_\mathrm{eq}} \tag{1}$$

TABLE III. Component values during simulation.

#	Description	L_s (H)	R_s (Ω)	R_eq (Ω)	τ (ms)
Sim 1	Ideal	1690	42.8	24.1	25000
Sim 2	Actual	1.69	42.8	24.1	25
Sim 3	Return to zero	0.133	42.8	24.1	2.0
Sim 4	Extreme	0.0133	42.8	24.1	0.2

B. Implications for Energy Metering

1) Simulation: In order to determine the implication of the CT response on energy metering, the product between the simulated CT response (i_ct) and an ideal 50 Hz sinusoidal voltage is processed in MATLAB, according to (2). The simulation uses a sampling rate of 25 MHz and a duration of 10 periods. This result is compared with the product between the input waveform (i_s) of the simulation and the ideal voltage, in order to find the energy error, according to (3). The current waveform is then phase shifted with respect to the ideal voltage from 0° till 180° to determine the relation between the phase shift of the pulse and the error, similarly to [11] when researching a Rogowski coil static energy meter. This approach relates to different dimmer settings of phase-firing dimmers that were found to cause interference on static energy meters before [25].

$$P_x = \sum_{n=0}^{N-1} i_x\,[n] \cdot v_x\,[n] \tag{2}$$

$$\Delta P = P_\mathrm{dut} - P_\mathrm{ref} \tag{3}$$

2) Measurement: The results obtained by the simulation model are verified with measurements of the static energy meter under test. This is done using the measurement setup as provided in Fig. 8, where an ac controlled-current load is used to draw the test waveforms, similar to [11] where a Rogowski coil based meter was researched. The source voltage is generated using a Pacific Power Smart Source 140-TMX, which is a four-quadrant ac voltage source. In order to prevent instability of the ac load and to reduce voltage transients during a fast $\mathrm{d}i/\mathrm{d}t$, a 10 µF capacitor is added to reduce the source impedance seen by the load and to allow for faster current pulses. It represents the C_x capacitors as used in a power systems, which is included in various standards (AECTP501, MIL-STD 461G). This capacitor has been added in front of the static energy meter under test such that the reactive current will not flow through the meter. The static energy meter under test was explained before in Section II. The voltage and current as sensed by the voltage divider and CT inside the meter are probed as is visualized in Fig. 3(a). The voltage (v_sm) and current (i_sm) which are input to the MCU are used, so the signal after the TIA in case of the CT is probed. These are probed using Cleverscope CS1001 passive probes, and connected to a Cleverscope CS448 isolated

oscilloscope. A sampling rate of 25 MHz is used and 10 periods are captured. To determine the power consumed by the static energy meter the product of the measured voltage and current is taken, according to (2). For reference, the voltage (v_{ref}) is measured using a Pico Technology TA043 differential voltage probe and the current (i_{ref}) is measured with a Keysight N2783B current probe, both with a bandwidth of 100 MHz. These are also connected to the Cleverscope CS448. To determine the reference power the product of the measured voltage and current is taken, according to (2). Then the (potential) error of the static energy meter is determined using (3). The ac controlled-current load is able to draw arbitrary currents, which enables the testing of static energy meters in a controllable manner by adjusting current waveform parameters. This is not possible with commercial off-the-shelf (COTS) equipment. A Teledyne T3AFG waveform generator is used to regulate the current waveforms drawn by the ac controlled-current load. The load is synchronized with the zero-crossing of the source voltage using a trigger. In order to verify the simulation the drawn current waveform is the same as the simulation test waveforms, and thus has an amplitude of 10 A, pulse width of 1 ms, and rise/fall times of 1 µs. The current is phase shifted with respect to the voltage from 15° till 150° in steps of 15°. Lower or higher phase firing angles could not be used due to limitations of the load.

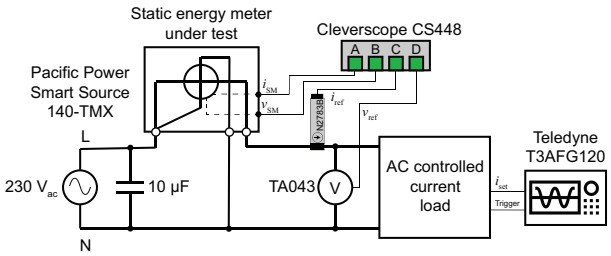

Fig. 8. Schematic overview of the used measurement setup.

V. Simulation of the CT Response

The response of the CT is simulated in order to find the root-cause of interference on static energy meters. Fig. 9 shows the response when a 50% square-wave is used as test waveform. For the ideal CT (*Sim 1*) the wave-shape is perfectly reconstructed, the time constant of the equivalent circuit is large enough to not affect the constant part of the square-wave. The only difference with the test waveform (in Fig. 7(a)) is the average value, which is 5 A for the test waveform and 0 A for the response of *Sim 1* due to its inability to measure the dc-offset. This will not cause any problems for energy metering, as the product of any dc value in the current with the mains voltage, that is mainly a 50 Hz sinusoidal voltage, will result in zero energy/power due to orthogonality [26]. For the other configurations of the CT, the constant part of the square-wave is not correctly reproduced and droop occurs. Where for *Sim 3* and *Sim 4* the current returns completely to zero after the rising edge before the falling edge starts. As the time constant is small compared to the constant part of the square-wave. For *Sim 2*, which represents the actual CT under test, the current drops 2 A in between the rising and falling edge, which is 20% of the rising edge value. Besides, the responses evidence that the fast rising/falling edge of the pulse is not causing any problems as it is perfectly reconstructed.

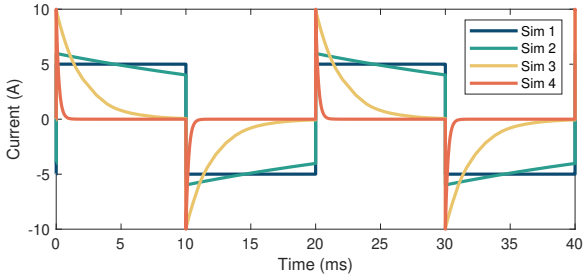

Fig. 9. Simulation of the CT response for *Wave 1*.

For the rest of the test waveforms the focus is on the results with *Sim 1* and *Sim 2* as it covers the ideal and actual CT circuit. Fig. 10 shows the simulation result for *Wave 2* which is a simplified representation of the interference waveform. Both at the top and bottom constant part the exponential decay based on the time constant is visible, similar to the response of *Wave 1*. For *Wave 3* a similar behavior is present for the bi-polar pulse, and therefore not shown. Lastly, *Wave 4* also shows the exponential decay when a sinusoidal is super-positioned at the constant part of the pulse, as is shown in Fig. 11 for *Sim 2*, when comparing *Wave 2* and *Wave 4*. This shows that the top-part of the pulse does not strictly have to be constant in order to observe the droop behavior. This is the case for a current waveform that is present in a real case where the static energy meter is placed in, for example the waveform provided in Fig. 1(a). This behavior is logically as in frequency-domain it is just an addition of a chopped 1 kHz sinusoidal, which can be measured perfectly fine by the CT, to the spectrum representing the pulsed current that caused the erroneous response.

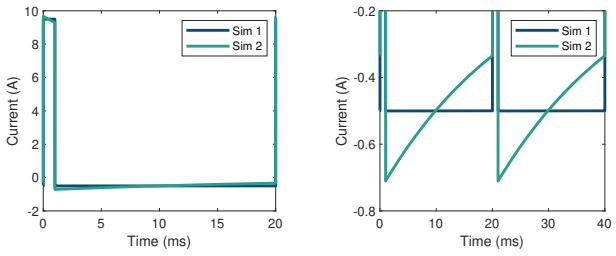

(a) Full response (b) Zoomed response

Fig. 10. Simulation of the CT response for *Wave 2*.

Overall, the simulation results show that the magnetization inductance (L_{e}) has a large effect on the response of the CT, even when considering the parameters of the actual CT. To limit the droop effects the time constant should be large compared to the pulse length to minimize the error. The effect of this inequality on energy metering is shown in the next section.

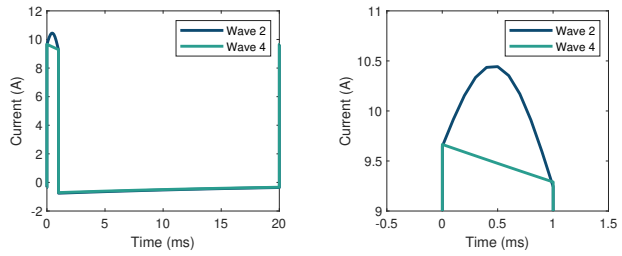

(a) Full response (b) Zoomed response

Fig. 11. Comparison of simulation *Sim 2* of the CT response for *Wave 2* and *Wave 4*.

VI. Implications for Energy Metering

A. Simulation

In order to determine the implications for energy metering only the simulation of the actual CT (*Sim 2*) is considered. The effect of changing the phase firing angle of the response of the CT with respect to the voltage is visualized in Fig. 12. This is similar to changing the phase firing angle of a dimmer, e.g. to change the intensity of a lamp, this was proven to affect static energy meters [25]. It should be noted that by phase shifting the current, the power drawn also changes. The highest power is drawn when the current pulse is fired exactly at the maximum value of the sinusoidal voltage. The simulation of the phase firing angle is shown in Fig. 13 for *Wave 2*, *Wave 3*, and *Wave 4*. It can be seen that changing the phase firing angle also changes the power error, where the highest absolute errors occur at 0° and 180°. This corresponds to the most dimming for a phase-firing dimmer (i.e. least power drawn). Similar errors occur for *Wave 2* and *Wave 4*, while for *Wave 3* (bi-polar pulse) the errors are doubled, which is logical as there are two rather than one pulse(s) present in the test waveform. The difference in current between the simulated response of the CT and the input signal is visualized in Fig. 14 for two different phase firing angles (0° and 162°). Besides, the figure shows whether the product between the voltage and current (and thus power error) is negative (red) or positive (green). These two plotted phase firing angles correspond to the phase firing angles of the signals plotted in Fig. 13. It shows the discrepancy at the constant part of the square-wave due to the exponential decay occurring (droop of the CT). When that difference in current is multiplied with the voltage in order to obtain the power it causes a negative or positive error dependent on where the pulse is placed with respect to the sinusoidal voltage due to symmetry, as is clearly visible by the red and green parts in Fig. 14. When the pulse is placed exactly under the maximum of the sinusoidal voltage ($\approx 90°$) the negative and positive error contributions are equal and thus do not cause any error. For phase firing angles smaller than $\approx 90°$ negative errors are expected, thus less power measured by the static energy meter than is actually consumed. For phase firing angles larger than $\approx 90°$ positive errors are expected based on the simulation results, so more power measured by the static energy meter than is actually consumed.

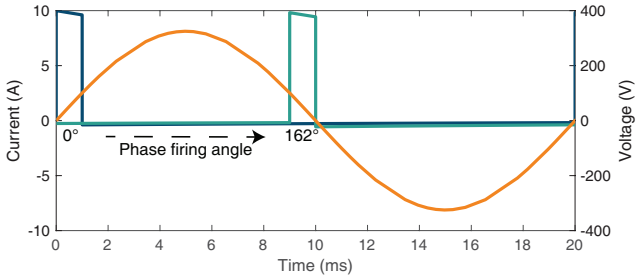

Fig. 12. Visual representation of phase firing of the current response of the CT relative to the ideal voltage.

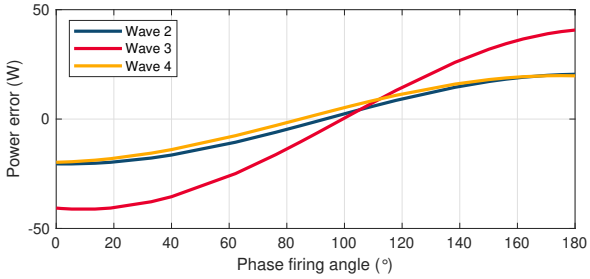

Fig. 13. Simulation of the power error for different phase firing angles.

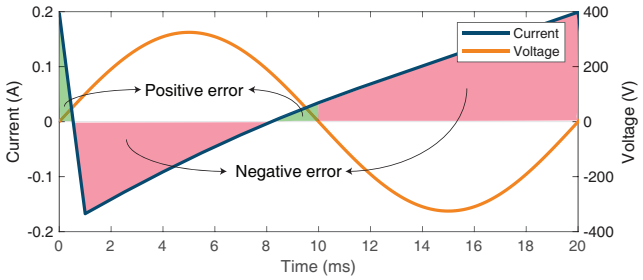

(a) Phase firing angle of 0°

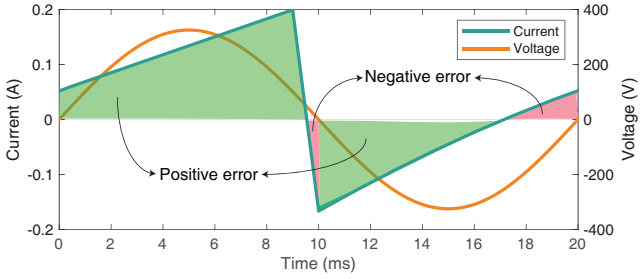

(b) Phase firing angle of 162°

Fig. 14. Difference between the current of the simulated response of the actual CT compared with the input signal, for different phase firing angles. It shows if the product between the voltage and current (and thus power error) is negative (red) or positive (green). This explains why the phase firing angle changes the power error from negative to positive.

B. Measurement

Next, the simulated results are confirmed with measurements. Only the results with the most simple test waveform, *Wave 2*, are provided as the previously conducted simulations show similar errors for the other test waveforms. First, the measured response inside the static energy meter is visualized in Fig. 15. The response looks very similar to the result of the

simulation in Fig. 10, except for the noise present. Besides, the amplitude of the exponential decay is slightly higher for the measurement (0.7 A) compared to the simulation (0.4 A). This means that the time constant is a bit smaller in practice compared to the simulation value.

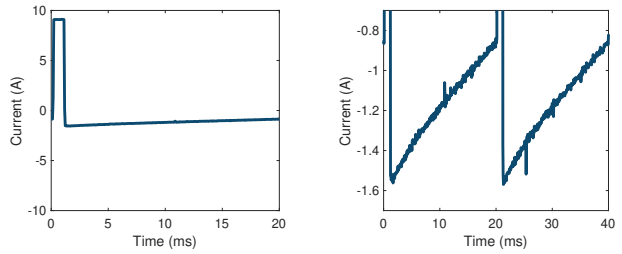

(a) Full response (b) Zoomed response

Fig. 15. Measured response of the CT inside the static energy meter.

Second, the pulsed waveform is phase shifted with respect to the voltage from 15° till 150° in steps of 15°. The power errors for different phase firing angles can be seen in Fig. 16. As expected the measured errors are higher than the simulated errors, as the measured response is also worse compared to the simulated response.

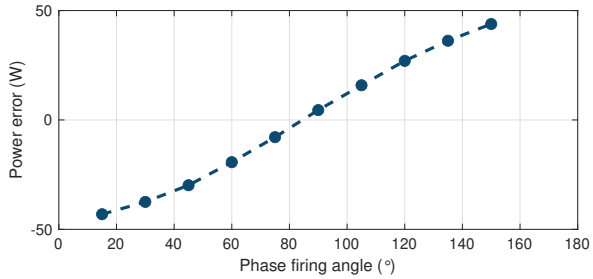

Fig. 16. Measurement of the power error for different phase firing angles.

These measurement results confirm the simulation result and show that interference of CT based static energy meters occur due to droop of the CT. It is evidenced that the phase firing angle correlates with the size of the error. Either under- or over-estimations of the energy consumption can occur based on the phase firing angle being smaller or larger than 90°, due to symmetry of the mains voltage. The errors are relevant as the correlation with the phase firing angle corresponds to appliances (e.g. luminaries) being dimmed. When the waveform is phase fired more, which is similar to an appliance being dimmed more, the interference increases. Furthermore, the test waveforms represent pulses found in actual installations, thus the EMI problem might be quite severe.

VII. Conclusion

This article shows that a discrepancy in the current response of CTs results in interfered energy consumption measurements by static energy meters. This occurs due to droop of the CT when measuring pulsed currents. These erroneous effects can be limited by a large time constant of the equivalent circuit. These errors are correlated to the phase firing angle of the pulse with respect to the voltage. When the current pulse is fired at the maximum of the voltage ($\approx 90°$) no errors occur, but when the pulse is fired either towards 0° or 180° the errors increase. This occurs for example when a dimmer is used to increasingly dim a luminary. For firing angles below 90° negative errors occur, so less consumption is measured by the static energy meter than is actually consumed. For firing angles above 90° positive errors occur, so more consumption is measured by the static energy meter than is actually consumed. This difference is due to symmetry of the mains voltage. The test waveforms represent pulsed currents found in actual installations, thus the EMI problem might be quite severe and impact energy bills of consumers. The results explain the root-cause for the interference of CT based static energy meters.

References

[1] Tounquet, Frédéric and Alaton Clément, "Benchmarking smart metering deployment in the EU-28 ," European Comission, Tech. Rep., 2020.

[2] A. Ari, N. Arregui, S. Black, O. Celasun, D. M. Iokova, A. Mineshima, V. Mylonas, I. W. H. Parry, I. Teodoru, and K. Zhunussova, "Surging Energy Prices in Europe in the Aftermath of the War: How to Support the Vulnerable and Speed up the Transition Away from Fossil Fuels," *IEWorking Paper No. 2022/152*, pp. 1–41, Jul. 2022.

[3] A. Cataliotti, V. Cosentino, and S. Nuccio, "Static Meters for the Reactive Energy in the Presence of Harmonics: An Experimental Metrological Characterization," *IEEE Transactions on Instrumentation and Measurement*, vol. 58, no. 8, pp. 2574–2579, Aug. 2009.

[4] P. Kotsampopoulos, A. Rigas, J. Kirchhof, G. Messinis, A. Dimeas, N. Hatziargyriou, V. Rogakos, and K. Andreadis, "EMC Issues in the Interaction Between Smart Meters and Power-Electronic Interfaces," *IEEE Transactions on Power Delivery*, vol. 32, no. 2, pp. 822–831, Apr. 2017.

[5] "Study Report on Electromagnetic Interference between Electrical Equipment/Systems in the Frequency Range Below 150 kHz," CLC/TR 50627, Tech. Rep., 2015.

[6] F. Leferink, C. Keyer, and A. Melentjev, "Static energy meter errors caused by conducted electromagnetic interference," *IEEE Electromagnetic Compatibility Magazine*, vol. 5, no. 4, pp. 49–55, Oct. 2016.

[7] B. ten Have, T. Hartman, N. Moonen, C. Keyer, and F. Leferink, "Faulty Readings of Static Energy Meters Caused by Conducted Electromagnetic Interference from a Water Pump," in *Renewable Energy and Power Quality Journal (RE&PQJ)*, Santa Cruz de Tenerife, Spain, 2019, pp. 15–19.

[8] T. Hartman, B. ten Have, N. Moonen, and F. Leferink, "How to Earn Money with an EMI Problem: Static Energy Meters Running Backwards," in *2021 Joint IEEE International Symposium on Electromagnetic Compatibility, Signal & Power Integrity, and EMC Europe*, Glasgow, United Kingdom, 2021, pp. 1–6.

[9] B. ten Have, M. A. Azpúrua, T. Hartman, M. Pous, N. Moonen, F. Silva, and F. Leferink, "Waveform Model to Characterize Time-Domain Pulses Resulting in EMI on Static Energy Meters," *IEEE Transactions on Electromagnetic Compatibility*, vol. 63, no. 5, pp. 1542–1549, Oct. 2021.

[10] S. Ziegler, R. C. Woodward, H. H.-C. Iu, and L. J. Borle, "Current Sensing Techniques: A Review," *IEEE Sensors Journal*, vol. 9, no. 4, pp. 354–376, Apr. 2009.

[11] T. Hartman, B. ten Have, J. Dijkstra, R. Grootjans, N. Moonen, and F. Leferink, "Susceptibility of Static Energy Meters due to Amplifier Clipping Caused by a Rogowski Coil," *IEEE Transactions on Electromagnetic Compatibility*, vol. 64, no. 6, pp. 2024–2032, Dec. 2022.

[12] B. ten Have, N. Moonen, and F. Leferink, "Electromagnetically Interfered Energy Metering Resulting from Droop of Current Transducers," in *2021 Joint IEEE International Symposium on Electromagnetic Compatibility, Signal & Power Integrity, and EMC Europe*, Glasgow, United Kingdom, 2021, pp. 1–5.

[13] K. Jain and P. Smith, "Fast-Rise-Time Pulse Transformers Built From Rotated Stacked 1:1 Transformers," *IEEE Transactions on Plasma Science*, vol. 34, no. 5, pp. 1853–1857, Oct. 2006.

[14] N. McNeill, N. K. Gupta, S. G. Burrow, D. Holliday, and P. H. Mellor, "Application of Reset Voltage Feedback for Droop Minimization in the Unidirectional Current Pulse Transformer," *IEEE Transactions on Power Electronics*, vol. 23, no. 2, pp. 591–599, Mar. 2008.

[15] B. ten Have, T. Hartman, N. Moonen, and F. Leferink, "Statistical Time-Domain Analysis of Equipment in Low-Voltage Networks," *IEEE Letters on Electromagnetic Compatibility Practice and Applications*, vol. 3, no. 4, pp. 114–117, Dec. 2021.
[16] B. ten Have, M. A. Azpúrua, T. Hartman, M. Pous, N. Moonen, F. Silva, and F. Leferink, "Estimation of Static Energy Meter Interference in Waveforms Obtained in On-Site Scenarios," *IEEE Transactions on Electromagnetic Compatibility*, vol. 64, no. 1, pp. 19–26, Feb. 2022.
[17] B. ten Have, T. Hartman, N. Moonen, and F. Leferink, "Static Energy Meters and the Electrical Environment Comply the Standards but Are Not Compatible," *IEEE Electromagnetic Compatibility Magazine [Manuscript accepted for publication]*, pp. 1–9, 2022.
[18] *Electricity metering equipment - Particular requirements - Part 21: Static meters for AC active energy (classes 0,5, 1 and 2)*, IEC 62053-21 b:2020 Std., 2020.
[19] *Electromagnetic Compatibility (EMC) - Part 4-19: Testing and measurement techniques - Test for immunity to conducted, differential mode disturbances and signalling in the frequency range from 2 kHz to 150 kHz, at a.c. power port*, IEC 61000-4-19 Std., 2014.
[20] B. ten Have, T. Hartman, N. Moonen, and F. Leferink, "Why Frequency Domain Tests Like IEC 61000-4-19 Are Not Valid; a Call for Time Domain Testing," in *2019 International Symposium on Electromagnetic Compatibility (EMC Europe 2019)*, Barcelona, Spain, 2019, pp. 124–128.
[21] A. Hargrave, M. J. Thompson, and B. Heilman, "Beyond the Knee Point : A Practical Guide to CT Saturation," in *2018 71st Annual Conference for Protective Relay Engineers (CPRE)*, College Station, TX, USA, 2018, pp. 1–23.
[22] W. H. Portilla, "Analysis of the non-linear behaviour of the magnetisation inductance during the frequency response test of a transformer," *IET Science, Measurement & Technology*, vol. 3, no. 8, pp. 1186–1193, Oct. 2019.
[23] S. Hodder, B. Kasztenny, N. Fischer, and Y. Xia, "Low Second-Harmonic Content in Transformer Inrush Currents - Analysis and Practical Solutions for Protection Security," in *2014 67th Annual Conference for Protective Relay Engineers*, College Station, TX, USA, 2014, pp. 705–722.
[24] B. ten Have, L. Bolzonella, T. Hartman, N. Moonen, and F. Leferink, "Susceptibility of Current Transformer Measurements Due to Pulsed Currents," in *2023 IEEE 7th Global Electromagnetic Compatibility Conference (GEMCCON)*, Bali, Indonesia, 2023, p. 1.
[25] Z. Marais, H. E. Van den Brom, G. Rietveld, R. Van Leeuwen, D. Hoogenboom, and J. Rens, "Sensitivity of static energy meter reading errors to changes in non-sinusoidal load conditions," in *2019 International Symposium on Electromagnetic Compatibility (EMC Europe 2019)*, Barcelona, Spain, 2019, pp. 202–207.
[26] T. Hartman, R. Grootjans, N. Moonen, and F. Leferink, "Electromagnetic Compatible Energy Measurements Using the Orthogonality of Nonfundamental Power Components," *IEEE Transactions on Electromagnetic Compatibility*, vol. 63, no. 2, pp. 598–605, April 2021.

Bas ten Have (Member, IEEE) received his B.Sc. degree in 2015, his M.Sc. degree in 2018, and his Ph.D. in 2022, all in electrical engineering, at the University of Twente, Enschede, The Netherlands. His M.Sc. and Ph.D. theses were related to electromagnetic interference on static energy meters.

Since 2021 he is a Researcher with the Power Electronics and Electromagnetic Compatibility Group, at the University of Twente. His research interests include low frequency EMI, EMC in power electronics and power systems, energy metering, and energy storage systems.

Dr. Ten Have is a member of the IEEE Electromagnetic Compatibility Society TC7 on low-frequency EMC and served as a reviewer for the IEEE Letters on Electromagnetic Compatibility Practice and Applications.

Leonardo Bolzonella received the B.Sc. degree in electrical engineering in 2022 from the University of Twente, Enschede, The Netherlands. His B.Sc. thesis was related to interfered responses of current transformers that are used for energy measurements inside static energy meters. Since 2022 he is working towards his M.Sc. degree in electric power engineering at the Technical University of Delft, Delft, The Netherlands.

Tom Hartman (Member, IEEE) received the B.Sc. and M.Sc. degree in electrical engineering in 2016 and 2018, respectively from the Group of Telecommunication Engineering, University of Twente, The Netherlands, where he has been working toward the Ph.D. degree in electromagnetic compatibility with the Power Electronics and Electromagnetic Compatibility Group, since August 2018.

Since August 2021, he has been a Lecturer with the same group. Mr. Hartman was the recipient of the 2021 President Memorial Award of the IEEE EMC Society.

Niek Moonen (Member, IEEE) received the B.Sc. degree in advanced technology, the M.Sc. in electrical engineering, and the Ph.D. (*cum laude*) degree in electromagnetic compatibility from the University of Twente, Enschede, The Netherlands, in 2012, 2014, and 2019, respectively.

Since January 2019, he has been with the Power Electronics and Electromagnetic Compatibility Group, University of Twente, first as a Senior Researcher and currently as an Assistant Professor. His research interests include electromagnetic interference (EMI) mitigation in power electronics with special interest in EMI propagation in smart grids, digital signal processing in electromagnetic compatibility measurements, and EMI filter optimization.

Dr. Moonen is a Member of the IEEE Electromagnetic Compatibility Society TC7 on low-frequency EMC, IEEE PELS society TC11 on aerospace power, TC12 on energy access and off-grid systems, and a Board Member of the Dutch EMC-ESD Association.

Frank Leferink (Fellow, IEEE) received his B.Sc in 1984, M.Sc. in 1992 and his PhD in 2001, all electrical engineering, at the University of Twente, Enschede, The Netherlands. He has been with THALES in Hengelo, The Netherlands since 1984 and is now the Technical Authority EMC. He is also manager of the Network of Excellence on EMC of the THALES Group, with over 100 EMC engineers scattered over more than 20 units, worldwide.

In 2003 he was appointed as (part-time, full research) professor, Chair for EMC at the University of Twente. At the University of Twente he lectures the course EMC, and manages several research projects, with 2 researchers and 15 PhD student-researchers. Over 300 papers have been published at international conferences or peer reviewed journals, and he holds 5 patents.

Prof. dr. Leferink is past-president of the Dutch EMC-ESD association, Chair of the IEEE EMC Benelux Chapter, member of ISC EMC Europe, member of the Board of Directors of the IEEE EMC Society, and associate editor of the IEEE Transactions on Electromagnetic Compatibility and the IEEE Letters on Electromagnetic Compatibility Practice and Applications.